



Assessing Methods and Data for Pore-Size Distribution of PEMFC Gas-Diffusion Media

Michael J. Martínez,^{a,*} Sirivatch Shimpalee,^{a,**} J. W. Van Zee,^{a,**,z} and A. V. Sakars^b

^aDepartment of Chemical Engineering, University of South Carolina, Columbia, South Carolina 29208, USA

^bPorotech Limited, Woodbridge, Ontario L4L 3Z5, Canada

Data for hydrophilic and hydrophobic pore-size distributions are presented for two gas-diffusion media (GDM) commonly used in proton exchange membrane fuel cells (PEMFCs). The data were obtained using two measurement methods, intrusion porosimetry and the method of standard porosimetry (MSP). The use of multiple working fluids to access hydrophilic and hydrophobic pores is discussed as well as limitations associated with structural changes of the GDM during the tests. The differences in the data between the two methods are discussed for both the carbon-cloth and carbon-paper GDM and it is shown that these differences have significant implications relative to the distribution of hydrophilic and hydrophobic pores that control liquid-water transport. The analysis presented in this work shows that the MSP can lead to a more consistent interpretation of the GDM structure for materials that are compressible.

© 2009 The Electrochemical Society. [DOI: 10.1149/1.3080653] All rights reserved.

Manuscript submitted July 17, 2008; revised manuscript received January 15, 2009. Published xx xx, xxxx.

Gas diffusion media (GDM) play a critical role in proton exchange membrane fuel cells (PEMFCs) by simultaneously providing several functions that minimize the voltage loss. The GDM must provide (i) good electronic conductivity to sustain electron flow between the catalyst layer and bipolar plates, (ii) good thermal conductivity to keep uniform temperature and efficient heat removal, (iii) mechanical strength to maintain good contact with the catalyst layer and bipolar plates without compressing into flow channels, (iv) good permeability that allows reactant gas distribution into the reaction sites, and (v) properties that allow liquid product water removal and prevent accumulation of a liquid-water film on the catalyst.

Common GDM consist of porous structures made from carbon-fiber paper or cloth,^{1,2} and in general, their bulk properties achieve functions *i*–*iv* above. However, to achieve function *v* and adjust the liquid-water removal for various operating conditions, the hydrophobicity of the GDM is increased by treatments with polytetrafluoroethylene (PTFE) or similar coatings. The hydrophobic treatment is usually obtained by dipping the GDM into an aqueous PTFE suspension.^{2,3} Although GDM manufacturers may have proprietary techniques to insure a complete and uniform hydrophobic structure, the structure is typically not specified and may include a combination of hydrophilic and hydrophobic pores. In addition, a microporous layer structure, usually consisting of a mixture of carbon particles with PTFE, is sometimes incorporated on the surface of the substrate to limit the loss of catalyst to the GDM interior and to help wick the liquid water away from the electrodes. These microlayers add to the complexity of the material, making it difficult to understand the key parameters for designing GDM. As a result, GDM formulations are found through rigorous trial-and-error methods,⁴⁻¹⁰ and much effort has been committed to develop two-phase models¹¹⁻¹⁵ and water-measurement techniques¹⁶ in order to understand the effect of liquid water in PEMFC.

Two-phase transport through GDM is affected by its morphology and ability to wet. The gas transport in the GDM is controlled by concentration gradients and the effective diffusion coefficient expressed as

$$D_{\text{am}}^{\text{eff}} = \frac{D_{\text{am}}}{N_M} \quad [1]$$

where D_{am} is the free-stream diffusion coefficient of species α in the mixture and N_M is the MacMullin number expressed as a func-

tion of the porosity (ϵ) and tortuosity (τ) of the pores¹⁷

$$N_M = f(\tau, \epsilon) \quad [2]$$

Local liquid transport is controlled by capillary action, where the capillary pressure is given by the Young–Laplace equation as

$$P_c = \frac{-2\sigma \cos \theta}{r} \quad [3]$$

In Eq. 3, the parameters σ , θ , and r are the surface tension, contact angle, and pore radius, respectively. On a global or volume-averaged description, the capillary pressure is commonly expressed in terms of liquid saturation (s_l) by means of the Leverett function.¹⁸⁻²³ Recent experimental measurements²⁴⁻²⁶ have focused on obtaining the empirical parameters for this function. As an alternative, which may be complimentary to these empirical methods, we study here methods that help understand the structure and pore-size distribution (PSD) in terms of the physical parameters shown in Eq. 1-3. As discussed below, these methods allow for measurement of the GDM structure and properties under PEMFC conditions (i.e., with temperature and compression stresses) in a way that may not be available with bulk average properties.

Although several techniques exist to characterize porous materials, there are two common techniques used to measure PSD and characterize the hydrophilic and hydrophobic nature of the pores for GDM. These techniques are intrusion porosimetry (IP)²⁷ and the method of standard porosimetry (MSP).²⁸ In this paper, the assumptions and the differences by which these two techniques access hydrophilic and hydrophobic pores are discussed. Two types of GDM, a carbon cloth and a carbon paper, are used to assess each technique in terms of its applicability under PEMFC conditions. Limitations associated with changes in the structure of the GDM during the tests are also discussed. Finally, the implications for the transport of liquid water in PEMFC are presented and discussed relative to the recent data and measurement techniques for the MacMullin number presented by Martínez et al.¹⁷ and Martínez.²⁹

Principles of the Methods

IP.— IP is a technique used to characterize the porosity of materials by applying different levels of pressure to the sample immersed in a working fluid. During the test, the pressure is controlled to force the fluid into the pores while the volume of the intruded fluid is measured. The pore size is obtained from Eq. 3 for each pressure applied assuming cylindrical pores. For nonwetting liquids (i.e., liquids that do not spontaneously fill the pores), this equation shows that smaller pores require higher pressures than larger pores for liquid intrusion. Consequently, as the pressure is gradually in-

* Electrochemical Society Student Member.

** Electrochemical Society Active Member.

^z E-mail: vanzee@enr.sc.edu

Table I. Parameters for the PSD techniques.

Entity	Working fluid	Surface tension (N/m)	Contact angle	Temperature (K)	Mechanical compression (kPa abs.)
IP-M					
PMI	Mercury	0.480	140°	Room Temp.	Vary as liquid intrude
Micromeritics	Mercury	0.485	130°	Room Temp.	Vary as liquid intrude
USC	Mercury	0.485	130°	Room Temp.	Vary as liquid intrude
IP-W					
PMI	Water	0.072	100°	Room Temp.	Vary as liquid intrude
MSP-O					
Porotech, Ltd.	Octane	0.022	0°	303	103 (No compression)
				323	531
MSP-W					
Porotech, Ltd.	Water	0.073	Vary	323	531

102 creased, the nonwetting liquid intrudes from larger to smaller pores.
 103 Typical pressures for mercury intrusion range from vacuum
 104 (~3.5 kPa) to about 417 MPa. The corresponding pore-diameter
 105 range depends on the contact angle and surface tension used in Eq.
 106 3. For mercury, the values $\theta_{\text{Hg}} = 140^\circ$ and $\sigma_{\text{Hg}} = 0.40$ N/m are typi-
 107 cally used for GDM, and thus the pore diameters range from 0.0035
 108 to about 420 μm . For water intrusion, the pressures range from
 109 vacuum to about 35 MPa and diameters from 0.0015 to 14 μm
 110 when $\theta_{\text{H}_2\text{O}} = 100^\circ$ and $\sigma_{\text{H}_2\text{O}} = 0.072$ N/m are used.
 111 Mercury is nonwetting for many materials. Consequently, IP with
 112 mercury as the working fluid (IP-M) is intended to access all the
 113 pores in the sample. Thus, an increment in pressure during the test is
 114 associated with an increment in volume of mercury intruded. This
 115 volume of mercury corresponds to the pore size intruded with the
 116 applied pressure. Conversely, water is wetting for the hydrophilic
 117 pores, and it spontaneously fills these pores without any applied
 118 pressure. Consequently, IP with water as the working fluid (IP-W) is
 119 intended to access hydrophobic pores in the sample. Thus, an incre-
 120 ment in pressure during the test is associated with an increment in
 121 volume of water intruded into the hydrophobic pores, and again,
 122 according to Eq. 2, this volume of water corresponds to the pore size
 123 at the applied pressure. Due to the pressure range, only the hydro-
 124 phobic pores from 0.0015 to 14 μm are accessed, and thus any hy-
 125 drophobic pores in the range from 14 to 420 μm are not measured.
 126 Details regarding the IP technique can be found elsewhere.²⁷

127 *MSP.*—The MSP, developed by Volfkovich et al.,²⁸ uses the
 128 principle of capillary equilibrium to characterize the porosity of ma-
 129 terials. When two materials partially saturated with a wetting liquid
 130 are placed in contact, the system moves toward equilibrium, which
 131 requires the capillary pressures to be equal. By placing the testing
 132 sample in contact with a standard sample (i.e., a sample with a
 133 known capillary pressure distribution), it is possible to obtain the
 134 capillary pressure associated with the amount of liquid in the test
 135 sample. By evaporating a small mass of the liquid, a new equilib-
 136 rium point can be determined. The MSP can measure pore diameters
 137 in the range of 0.0005–1500 μm with Eq. 2, a cylindrical pore as-
 138 sumption, and the parameters in Table I.
 139 Octane is wetting for most of the materials, and MSP with octane
 140 as the working fluid (MSP-O) is intended to access all the pores in
 141 the sample. Thus, each equilibrium pressure is associated to a total
 142 volume of octane measured. This volume of octane corresponds to
 143 the volume of the pores up to the pore size obtained from that
 144 equilibrium pressure. As described above, water is wetting for the
 145 hydrophilic pores. Consequently, MSP with water as the working
 146 fluid (MSP-W) is intended to access the hydrophilic pores in the
 147 sample. Thus, each equilibrium pressure is associated to a total vol-
 148 ume of water measured in the hydrophilic pores only. This volume
 149 of water corresponds to volume of the pores up to the pore size
 150 obtained from that equilibrium pressure.

Experimental

151

Materials.—The GDM materials selected for this work were
 Carbel CL from W. L. Gore and Associates, Inc., and Pyrofil MFG-
 070 from Mitsubishi Rayon Co., Ltd. Carbel CL is a woven carbon-
 cloth GDM with a micropore layer. Figure 1 shows scanning elec-
 tron microscope (SEM) images of the materials and the macrocracks
 in the micropore layer of Carbel CL. The micropore layer composi-
 tion was not analyzed due to proprietary agreements. The total un-
 compressed thickness is 406 μm . Conversely, Pyrofil is a carbon-
 paper GDM with an uncompressed thickness of 178 μm . Pyrofil
 does not have a micropore layer.

Measurements.—The PSD was measured for both GDM above
 using IP and MSP with their respective working fluids. For Carbel
 CL, the IP-M measurements were performed at Porous Materials,
 Inc. (PMI), Micromeritics Instrument Corporation, and the Univer-
 sity of South Carolina (USC) with Micromeritics equipment. Only
 the IP-W measurements were performed at PMI. The parameters
 used by each entity are listed in Table I. For Pyrofil, the IP-M and
 IP-W measurements were performed at PMI. Measurements using
 MSP-O and MSP-W were performed by Porotech, Ltd. The param-
 eters used are also listed in Table I. For Carbel CL, the measure-
 ments were performed at uncompressed and compressed conditions
 used in PEMFCs (i.e., 343 K and 531 kPa compression).

Results and Discussion

174

Figure 2 compares the integral porometric curves for Carbel CL
 using IP-M and MSP-O as well as the reproducibility (or inherent
 variability) in the IP-M data. As explained above, the pressure ap-
 plied during the IP-M test increases from vacuum (~3.6 kPa as
 shown in the lower right corner of Fig. 2) as mercury intrudes into

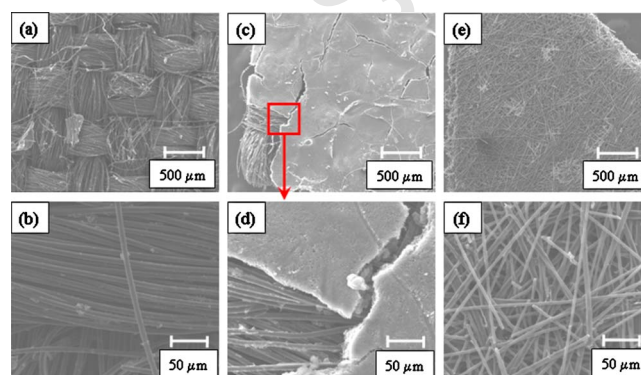


Figure 1. (Color online) SEM images of Carbel CL macropore layer (a and b) and micropore layer (c and d) and Pyrofil macropore layer (e and f). Pyrofil does not have a micropore layer.

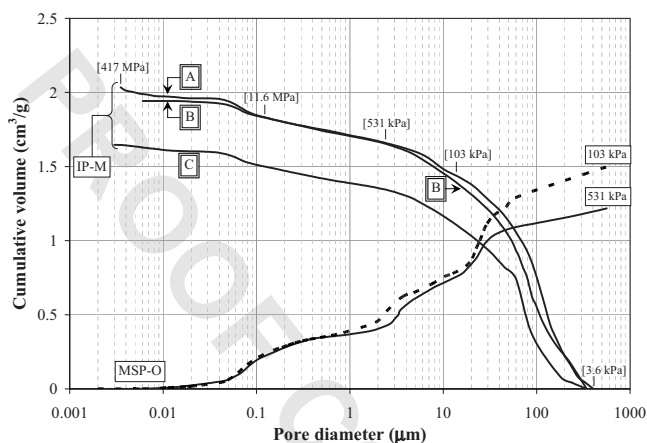


Figure 2. Comparison of integral porometric curves for Carbel CL using IP-M and MSP-O. IP-M curves correspond to PMI (A), USC (B), and Micromeritics (C). The pressure for IP-M tests varies from 3.6 kPa to 417 MPa. Brackets indicate pressures applied for the IP measurements at the respective diameters and volumes. The pressure for MSP-O is constant at 103 (---) and 531 kPa (—).

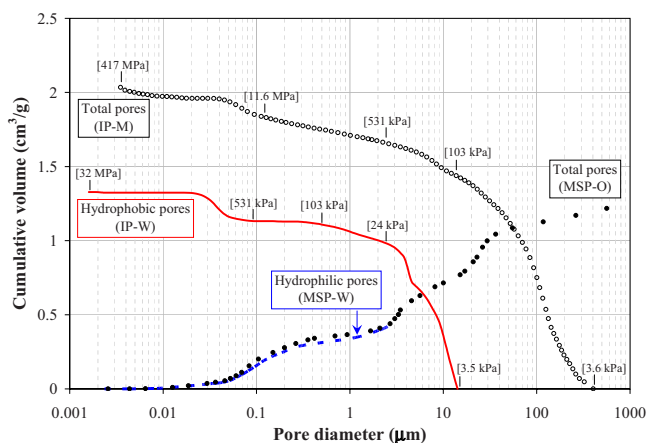


Figure 3. (Color online) Comparison of integral porometric curves of hydrophilic and hydrophobic pores for Carbel CL using IP-W and MSP-W. Brackets indicate pressures applied for the IP measurements at the respective diameters and volumes. The MSP-W and MSP-O curves were obtained at 531 kPa. The hydrophilic curve for MSP-W ends at 2.5 μm (0.42 cm^3/g). Legend: IP-M (\circ), IP-W (—), MSP-O (\bullet), MSP-W (---).

180 smaller pores from the large-diameter pores. Because Carbel CL is a
 181 soft carbon cloth, high pressures deform or compress the pores that
 182 have not been intruded by mercury. Conversely, the MSP test is
 183 performed under constant compression of the GDM, allowing mea-
 184 surement of the total pore volume at a specified compression of the
 185 GDM that may be consistent with an assembled fuel cell. This figure
 186 also shows the MSP test performed with octane at 103 and 531 kPa,
 187 pressures which were selected to compare the uncompressed GDM
 188 (at 101 kPa) and the GDM compressed in fuel cells assembled at
 189 USC. Consequently, the curve at 531 kPa shows a lower total pore
 190 volume due to compression of the pores in the macropore region.
 191 The micropores were not compressed.

192 Tick marks on the IP-M curves are located at the points where
 193 the pressure has reached 103 and 531 kPa. Because the pressure
 194 increases gradually in the IP-M technique, the cumulative volume
 195 measured up to 531 kPa (i.e., 1.65 cm^3/g for curves A and B and
 196 1.34 cm^3/g for curve C) is higher than the cumulative volume mea-
 197 sured with MSP-O at 531 kPa (i.e., 1.22 cm^3/g). Consequently, the
 198 final cumulative volume for the IP-M is higher than that for the
 199 MSP-O. However, we cannot explain the larger volume in the IP-M
 200 curves at 417 MPa as compared to the MSP-O curve at 103 kPa, if
 201 we assume that the final cumulative volume of the MSP-O at
 202 103 kPa is the correct total pore volume of the GDM. However, if
 203 we assume that more volume is accessible due to the higher pressure
 204 in the IP-M, we must conclude that the MSP-O at 103 kPa does not
 205 correspond to the total pore volume of the GDM. Alternatively, one
 206 might argue that the additional volume is not accessible under
 207 PEMFC applications because the internal compressions of the GDM
 208 are in the 700 kPa range.

209 Measured integral porometric curves of hydrophilic and hydro-
 210 phobic pores for Carbel CL are shown in Fig. 3. Again, different
 211 working fluids are used to obtain the PSD for each pore type; for
 212 that reason, with water, hydrophobic pores are measured by the
 213 IP-W technique and hydrophilic pores are measured with the
 214 MSP-W technique. For the IP-M technique, the total pore volume,
 215 including hydrophilic and hydrophobic pores, measured by PMI was
 216 2.03 cm^3/g (at a pore diameter of $\sim 0.003 \mu\text{m}$). PMI also measured
 217 the total hydrophobic pore volume using IP-W as 1.33 cm^3/g (at a
 218 pore diameter of $\sim 0.002 \mu\text{m}$), but this number is unrealistic for two
 219 reasons. First, the hydrophobic pore volume in the range from
 220 14 to 420 μm cannot be determined, as described previously, be-
 221 cause a vacuum corresponding to 0.119 kPa would be needed to
 222 start measuring hydrophobic pore volume at 420 μm , and the mini-
 223 mum vacuum in the IP-W test was 3.5 kPa. Second, the volume of

water intruded in the GDM between pore diameters of 2.1–14 μm is
 0.99 cm^3/g , which is greater than the volume of mercury intruded
 (0.25 cm^3/g) in the same pores. One explanation for this discrep-
 anomaly may be the compressibility of Carbel CL. That is, the pressure
 required to intrude mercury between pore diameters of 2.1–14 μm
 changes from 103 to 531 kPa, while the required pressures to intru-
 de water in the same pores varies from 3.5 and 24 kPa. Between
 103 and 531 kPa, Carbel CL would be compressed gradually. How-
 ever, between 3.5 and 24 kPa (about 1/4 atmospheric pressure), Car-
 bel CL does not compress, resulting in a change of slope with water
 intrusion, as observed in Fig. 3, due to the larger volume available.
 The MSP does not show these limitations. Hence, we recommend
 that the MSP-O be used for this material at 531 kPa to report the
 total pore volume, including hydrophilic and hydrophobic pores,
 which was measured as 1.22 cm^3/g . The total hydrophilic pore vol-
 ume measured with the MSP-W for the sample at 531 kPa psi was
 0.42 cm^3/g . This represents 34% of the total pores as hydrophilic
 (66% hydrophobic).

The analysis of the integral porometric curve for MSP-W shown
 in Fig. 3 is better shown in Fig. 4a, where the hydrophilic pore
 volume is subtracted from the total pore volume. There, the MSP-W
 allocates hydrophilic pores only below 2.5 μm and the hydrophobic
 pores exist only from 2.5 to 400 μm . The constant line after 2.5 μm
 in the hydrophilic curve indicates that there is no increase in the
 hydrophilic pore volume. The hydrophobic curve in the small pore
 range corresponds to less than 4% of the total pore volume and
 might be better described as experimental variance. Also, Fig. 4b
 shows the porometric curves for the differential distributions. From
 Fig. 4b, the volume associated to each pore size can be appreciated.
 The area under the curve for a specific pore-size range represents the
 volume associated with that range. However, because the curve is
 plotted in a logarithmic scale, an area in the region of larger pores
 represents a larger volume when compared to a similar area in the
 region of smaller pores. This figure shows a higher hydrophilic vol-
 ume around pores of 0.1 μm and higher hydrophobic volume
 around pores of 3.5 and 26.4 μm .

Figure 5 compares the integral porometric curves for Pyrofil us-
 ing IP-M and MSP-O. In this case, Pyrofil, a carbon-paper GDM,
 consists of a more firm structure than a carbon-cloth GDM, and
 consequently, deformations or pore compressions are less likely. Al-
 though the IP-M method reaches a pressure of about 416 MPa,
 which could compress empty pores, Fig. 5 shows that the mercury
 has already intruded 87% of the GDM pore volume at 531 kPa (i.e.,
 total volume equals 1.55 and 1.35 cm^3/g at 416 MPa and 531 kPa,

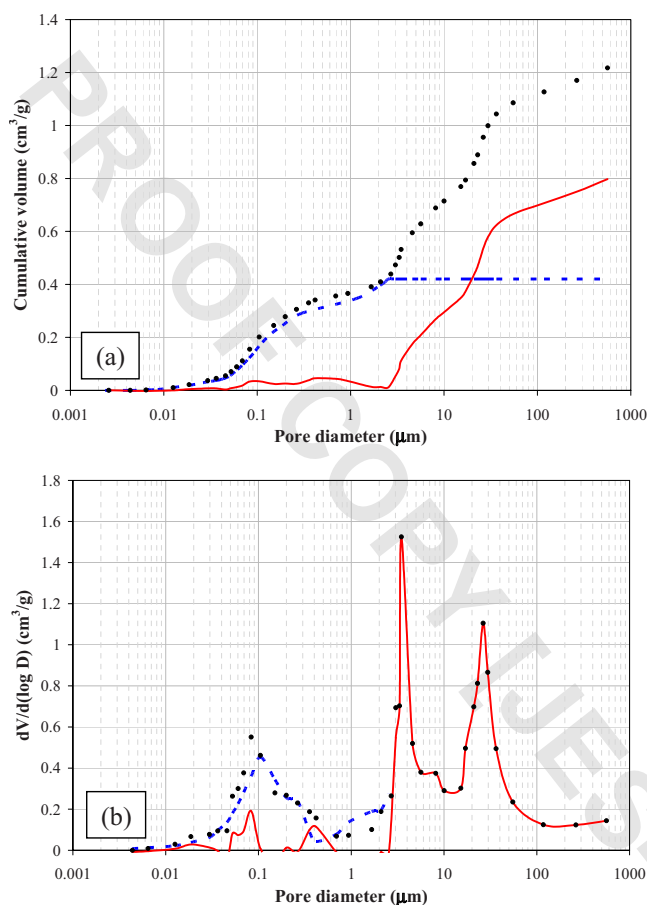


Figure 4. (Color online) Porometric curves for integral (a) and differential (b) distribution for Carbel CL at 531 kPa using MSP. Legend: total pores from MSP-O data (●), hydrophilic from MSP-W data (---), hydrophobic pores by subtraction (—).

268 respectively). Hence, any compression of the remaining empty pores
269 would be negligible. Also, both curves show the same total volume
270 (to within 3%), which is expected for a material that does not show
271 deformation due to compression. Again, this is not true for carbon-
272 cloth GDM, because it starts to compress at low pressures.

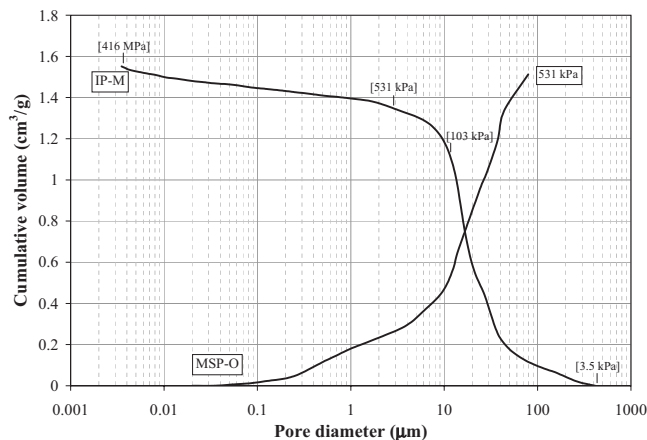


Figure 5. Comparison of integral porometric curves for Pyrofil using IP-M and MSP-O. IP-M curves correspond to PMI. The pressure for IP-M test varies from 3.5 kPa to 416 MPa. Brackets indicate pressures applied for the IP measurements at the respective diameters and volumes. The pressure for MSP-O is constant at 531 kPa.

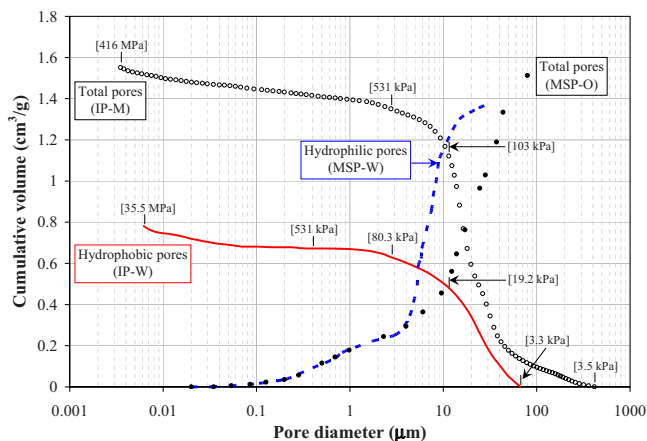


Figure 6. (Color online) Comparison of integral porometric curves of hydrophilic and hydrophobic pores for Pyrofil using IP-W and MSP-W. Brackets indicate pressures applied for the IP measurements at the respective diameters and volumes. The MSP-W and MSP-O curves were obtained at 531 kPa. The y-shifted IP-W curve assumes that all pores greater than 67 μm are hydrophobic. Legend: IP-M (○), IP-W (—), MSP-O (●), MSP-W (---).

Integral porometric curves of hydrophilic and hydrophobic pores
for Pyrofil are shown in Fig. 6. The total pore volume, including
hydrophilic and hydrophobic pores, measured by the IP-M techni-
que was 1.55 cm^3/g , while the total hydrophobic pore volume
using IP-W was measured as 0.78 cm^3/g . Again, the hydrophobic
pore volume in the range from 67 to 415 μm cannot be determined,
because the minimum vacuum pressure in the IP-W test was
3.3 kPa. However, if the pores between 67 and 415 μm are assumed
as hydrophobic, then the IP-W curve can be shifted by 0.13 cm^3/g ,
as shown in Fig. 6. Note that the volume changes in the IP-W curve
are equal to or lower than the volume changes in the IP-M curves,
and consequently, the hydrophobic pore volume for this shift is al-
ways equal to or below the total pore volume for any specified pore
range. In this way, the apparent total hydrophobic pore volume is
0.91 cm^3/g (i.e., 0.78 + 0.13 cm^3/g), representing 59% of the pore
volume as hydrophobic. When the MSP-O data at 531 kPa was
compared, the total pore volume, including hydrophilic and hydro-
phobic pores, was measured as 1.51 cm^3/g . This is in close agree-
ment with the IP-M method and, again, gives some confidence that
this material does not compress substantially. Unfortunately, the
MSP-W method appears to yield an unrealistic volume measurement
as indicated by a larger volume than the MSP-O measurement for
diameters greater than 4 μm . This may be because the Pyrofil ma-
terial (and perhaps other cellulosic or cotton-based materials) has a
tendency to expand or swell in water. While this expansion creates a
discrepancy in Fig. 6, the MSP-W method may provide some insight
to the expansion tendency when this material is exposed to water
during PEMFC operation. We express this as a tendency, because
the GDM is constrained by other soft goods and the bipolar plates.
This unrealistic PSD for the hydrophilic pores measured by the
MSP-W method is shown in Fig. 7. That is, the MSP-W curve is
shifted to the left of the MSP-O curve in Fig. 7a, and we label this
as unrealistic because the data for the MSP-W method should not
yield a larger value of the total volume than that measured by the
MSP-O method at any pore diameter. This shift is not caused by
pore compression, because, as discussed above, IP-M and the
MSP-O methods give a total volume that differs by less than 3%
even though the pressure is increased from 531 kPa to 416 MPa.
Again, this discrepancy can be discussed by recalling that the MSP
procedures use the affinity of water to determine the hydrophilic
PSD, and this affinity can be increased when the liquid infiltrates the
material and increases the pore volume. In Fig. 7a, we correct for
this swelling, observed after a pore diameter of 4 μm , by moving

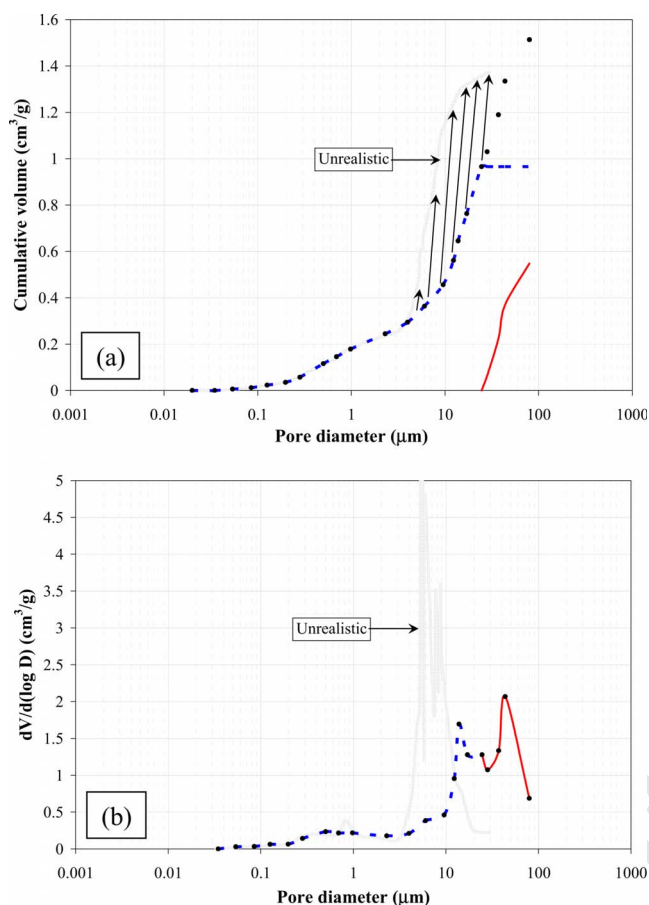


Figure 7. (Color online) Porometric curves for integral (a) and differential distribution (b) for Pyrofil at 531 kPa using MSP. Legend: total pores from MSP-O data (●), hydrophilic from MSP-W data labeled unrealistic (gray line), hydrophilic pores corrected for swelling (---), hydrophobic pores by subtraction (—).

316 the integral curve for hydrophilic pores (MSP-W) so it matches the
 317 integral curve for total pores (MSP-O). Consequently, the arrows in
 318 Fig. 7a show a possible scenario of the pore swelling in which the
 319 curve after the pores expand shows a higher cumulative volume
 320 corresponding to pores that now have a larger size. The dashed line
 321 represents the curve for hydrophilic pores after correcting for swell-
 322 ing, and it becomes horizontal at 25 μm , instead of 30 μm , because
 323 the expected curve for hydrophilic pores ends at a pore size that is
 324 smaller than the size corresponding to the integral curve for hydro-
 325 philic pores after swelling (i.e., the MSP-W curve). For this calcu-
 326 lation, where the dashed line corresponds to the hydrophilic pores
 327 before swelling, the solid line after 25 μm represents the hydropho-
 328 bic pores. With this scenario, Fig. 7b shows the porometric curves
 329 for the differential distribution where the hydrophilic and hydro-
 330 phobic pore distribution correspond to portions of the differential
 331 distribution of the total pores.

332 Although both the IP and MSP techniques show the same total
 333 volume for Pyrofil, and despite the possible swelling obtained in the
 334 MSP-W curve, the information obtained regarding the PSD of hy-
 335 drophobic and hydrophilic pores is different. From Fig. 6 it can be
 336 observed that increases in the integral porometric curve for IP-W
 337 fall between 0.06–0.006 and 67–1 μm , and thus these regions in-
 338 clude hydrophobic pores. The MSP-W data show that all of the
 339 pores less than 30 μm are hydrophilic and those between 30 and
 340 415 μm are hydrophobic. Thus, as with Carbel CL, the two methods
 341 yield different hydrophilic and hydrophobic PSD.

342 In an attempt to explain these differences, consider Fig. 8, which
 343 shows a schematic for two pores where the center sections are

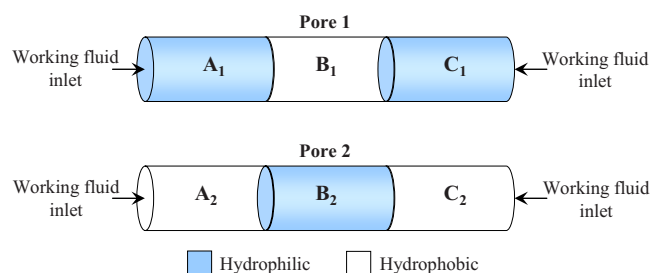


Figure 8. (Color online) Schematic of a pore with a hydrophobic section shielded by two hydrophilic sections (pore 1) and a pore with a hydrophilic section shielded by two hydrophobic sections (pore 2).

344 shielded by hydrophilic or hydrophobic pore sections. Assuming
 345 that the pore sections are not interconnected by other pores, we can
 346 predict the results that will be obtained by each PSD method as
 347 summarized in Table II. Recall that IP-M and the MSP-O techniques
 348 are intended to access all the pores, the IP-W is intended to access
 349 the hydrophobic pores, and the MSP-W is intended to access the
 350 hydrophilic pores, and that hydrophilic pores are obtained by sub-
 351 traction in the IP method while hydrophobic pores are obtained by
 352 subtraction with the MSP. In theory, as long as the method does not
 353 change the pore structure (e.g., pore compression or expansion), the
 354 IP-M and the MSP-O should access the same total volume for pores
 355 1 and 2. Also, for pore 1, the IP-W and the MSP-W techniques will
 356 access correctly the hydrophobic and hydrophilic sections, respec-
 357 tively. However, for pore 2, the IP-W method will overestimate the
 358 hydrophobic volume by the same amount that the MSP-W underesti-
 359 mates the hydrophilic volume. That is, the IP-W and MSP-W tech-
 360 niques will lead to the same erroneous conclusion that pore 2 is
 361 completely hydrophobic.

362 Now, let us consider GDM with pores that are interconnected by
 363 other hydrophilic or hydrophobic sections. Figure 9 shows the same
 364 type of pores presented in Fig. 8 but with interconnections. The
 365 analysis for these pores is also summarized in Table II, and the
 366 conclusions are the same. For these pores, the IP-M and the MSP-O
 367 should access the total volume. For pores 3 and 4, the IP-W and the
 368 MSP-W techniques access correctly the hydrophobic and hydro-
 369 philic sections, respectively. However, for pores 5 and 6, the IP-W
 370 method overestimates the hydrophobic volume by the same amount
 371 that the MSP-W underestimates the hydrophilic volume. Again, the
 372 IP-W and MSP-W techniques lead to the same erroneous conclusion
 373 that pores 5 and 6 are completely hydrophobic.

374 From this analysis, one can understand that pores with hydropho-
 375 bic sections completely shielded by hydrophilic sections have the
 376 correct assignment of the hydrophilic and hydrophobic volume with
 377 either technique (IP-W or MSP-W). However, if several combined
 378 sections (hydrophilic and hydrophobic) are completely shielded by
 379 hydrophilic sections, then the IP-W method overestimates the hy-
 380 drophobic volume by the same amount that the MSP-W underesti-
 381 mates the hydrophilic volume. Pores with hydrophilic sections com-
 382 pletely shielded by hydrophobic sections result in the erroneous
 383 assignment of the volume measured as hydrophobic with either
 384 technique (IP-W or MSP-W). This may be why Fig. 3 and 4 show
 385 no hydrophilic pores above 2.5 μm . This explanation for discrepan-
 386 cies can now be added to previous observations for the IP
 387 technique,²⁷ in which the volume measured for the wide parts of a
 388 nonuniform pore accessed through constricted parts of the pore is
 389 attributed to the constricted part of the pore. Consequently, pore
 390 configurations where wider parts are accessed through constricted
 391 parts in combination with hydrophilic and hydrophobic sections re-
 392 sult in PSD disagreement, as discussed in this work.

Table II. Results produced by the IP and MSP methods when accessing the pores shown in Fig. 8 and Fig. 9.

PSD Method	Expected Volume	Volume Measured	Comments
All pore case			
MSP-O	All	All	Wets complete pore
IP-M	All	All	Intrudes complete pore
Pore 1 (hydrophobic section shielded by hydrophilic sections)			
MSP-W	$A_1 + C_1$	$A_1 + C_1$	Correctly wets hydrophilic sections
IP-W	B_1	B_1	Correctly intrude hydrophobic section
Pore 2 (hydrophilic section shielded by hydrophobic sections)			
MSP-W	B_2	0	Underestimate hydrophilic volume by B_2
IP-W	$A_2 + C_2$	$A_2 + B_2 + C_2$	Overestimate hydrophobic volume by B_2
Pore 3 (hydrophobic section shielded by hydrophilic sections; hydrophilic sections interconnected by hydrophilic pore)			
MSP-W	$A_3 + C_3 + D_3$	$A_3 + C_3 + D_3$	Correctly wets hydrophilic sections
IP-W	B_3	B_3	Correctly intrude hydrophobic section
Pore 4 (hydrophobic section shielded by hydrophilic sections; hydrophilic sections interconnected by hydrophobic pore)			
MSP-W	$A_4 + C_4$	$A_4 + C_4$	Correctly wets hydrophilic section
IP-W	$B_4 + D_4$	$B_4 + D_4$	Correctly intrude hydrophobic sections
Pore 5 (hydrophilic section shielded by hydrophobic sections; hydrophobic sections interconnected by hydrophilic pore)			
MSP-W	$B_5 + D_5$	0	Underestimate hydrophilic volume by $B_5 + D_5$
IP-W	$A_5 + C_5$	$A_5 + B_5 + C_5 + D_5$	Overestimate hydrophobic volume by $B_5 + D_5$
Pore 6 (hydrophilic section shielded by hydrophobic sections; hydrophobic sections interconnected by hydrophobic pore)			
MSP-W	B_6	0	Underestimate hydrophilic volume by B_6
IP-W	$A_6 + C_6 + D_6$	$A_6 + B_6 + C_6 + D_6$	Overestimate hydrophobic volume by B_6

393

Conclusions

394 This work provided an overview for the interpretation of PSD
395 data for carbon-cloth and carbon-paper GDM obtained from IP and
396 MSP techniques. The advantages and limitations discussed in this
397 work are summarized below.

398 The IP technique has several limitations with both working flu-
399 ids, mercury and water. The high pressure applied for fluid intrusion
400 leads to compression of the structure of soft GDM. The use of a
401 constant contact angle can result in a wrong calculation of the pore
402 size for a measured pressure and volume. Volume measured in wider

parts of pores that are accessed through constricted parts are incor-
rectly attributed to the pore size corresponding to the constricted
part.²⁷ The IP-W technique is limited by the pore-size range that can
be measured, resulting in incomplete information of hydrophobic
pores. The IP-W technique overestimates the hydrophobic pore vol-
ume of pores containing hydrophilic sections shielded by hydropho-
bic sections.

The MSP technique offers several advantages over the IP techni-
que. Tests with MSP can be performed under constant compression
of the GDM and over a wide pore-size range with both octane
and water. The fact that octane has a contact angle of zero for most
materials decreases experimental errors associated with contact-
angle variations and distributions. When water is used, the MSP
technique accounts for variations in contact angle. The disadvantage
of MSP-W is that it cannot correctly measure the hydrophilic pore
volume in materials that swell. Also, the MSP-W underestimates the
hydrophilic pore volume of pores containing hydrophilic sections
shielded by hydrophobic sections.

The analysis presented in this work shows that MSP can be used
to understand the structure of GDM that can be found under PEMFC
conditions. In the future, this method coupled with modeling may
allow prediction of the required ratio of hydrophobic to hydrophilic
pores for various nonflooding operating conditions.

Acknowledgments

This research was supported by the National Science Foundation
of Industrial/University Collaborative Research Center for Fuel
Cells (EEC-0324260). Author M.J.M. was supported in part by a
scholarship (HRD-0450279) from the Southeast Alliance for Gradu-
ate Education and the Professoriate and by the Alfred P. Sloan Foun-
dation during the completion of this work. The authors also ac-
knowledge the helpful discussions with Professor Y. M. Volfkovich,
who is part of Porotech, Ltd., and the A. N. Frumkin Institute of
Physical Chemistry and Electrochemistry of the Russian Academy
of Sciences, Moscow, 119991, Russian Federation.

University of South Carolina assisted in meeting the publication costs of
this article.

References

1. A. L. Dicks, *J. Power Sources*, **156**, 128 (2006).
2. M. F. Mathias, J. Roth, J. Fleming, and W. Lehnert, in *Handbook of Fuel Cells—
Fundamentals, Technology and Applications*, W. Vielstich, H. A. Gasteiger, and A.
Lamm, Editors, pp. 517–537, John Wiley & Sons, New York (2003).

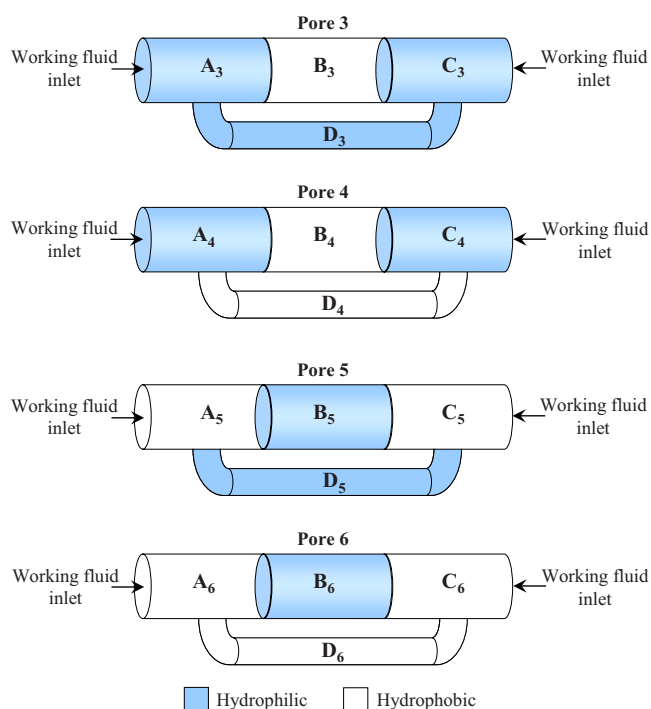


Figure 9. (Color online) Schematic of pores with hydrophilic and hydrophobic sections where some sections are interconnected by other hydrophilic or hydrophobic pores.

- 445 3. Y. M. Volkovich, V. E. Sosenkin, N. F. Nikolskaya, and T. L. Kulova, *Russ. J. Electrochem.*, **44**, 278 (2008). 467
- 446 4. W. K. Lee, C. H. Ho, J. W. Van Zee, and M. Murthy, *J. Power Sources*, **84**, 45 (1999). 468 AQ:
- 447 5. E. Passalacqua, G. Squadrito, F. Lufrano, A. Patti, and L. Giorgi, *J. Appl. Electrochem.*, **31**, 449 (2001). 469 #2
- 448 6. G. G. Park, Y. J. Sohn, T. H. Yang, Y. G. Yoon, W. Y. Lee, and C. S. Kim, *J. Power Sources*, **131**, 182 (2004). 470
- 449 7. C. Lim and C. Y. Wang, *Electrochim. Acta*, **49**, 4149 (2004). 471
- 450 8. H. K. Atiyeh, K. Karan, B. Peppley, A. Phoenix, E. Halliop, and J. Pharoah, *J. Power Sources*, **170**, 111 (2007). 472
- 451 9. G. Selvarani, A. K. Sahu, P. Sridhar, S. Pitchumani, and A. K. Shukla, *J. Appl. Electrochem.*, **38**, 357 (2008). 473
- 452 10. S. Park, J. W. Lee, and B. N. Popov, *J. Power Sources*, **177**, 457 (2008). 474
- 453 11. C. Y. Wang, *Chem. Rev. (Washington, D.C.)*, **104**, 4727 (2004). 475
- 454 12. A. Z. Weber and J. Newman, *Chem. Rev. (Washington, D.C.)*, **104**, 4679 (2004). 476
- 455 13. A. Biyikoglu, *Int. J. Hydrogen Energy*, **30**, 1181 (2005). 477
- 456 14. W. Q. Tao, C. H. Min, X. L. Liu, Y. L. He, B. H. Yin, and W. Jiang, *J. Power Sources*, **160**, 359 (2006). 478
- 457 15. C. H. Min, Y. He, X. L. Liu, B. H. Yin, W. Jiang, and W. Q. Tao, *J. Power Sources*, **160**, 374 (2006). 479
- 458 16. J. St-Pierre, *J. Electrochem. Soc.*, **154**, B724 (2007). 480
17. M. J. Martínez, S. Shimpalee, and J. W. Van Zee, *J. Electrochem. Soc.*, In press. 481
18. C. Y. Wang and P. Cheng, *Adv. Heat Transfer*, **30**, 93 (1997). 482
19. U. Pasaogullari and C. Y. Wang, *J. Electrochem. Soc.*, **151**, A399 (2004). 483
20. E. C. Kumbur, K. V. Sharp, and M. M. Mench, *J. Power Sources*, **168**, 356 (2007). 484
21. E. C. Kumbur, K. V. Sharp, and M. M. Mench, *J. Electrochem. Soc.*, **154**, B1295 (2007). 485
22. E. C. Kumbur, K. V. Sharp, and M. M. Mench, *J. Electrochem. Soc.*, **154**, B1305 (2007). 486
23. E. C. Kumbur, K. V. Sharp, and M. M. Mench, *J. Electrochem. Soc.*, **154**, B1315 (2007). 487
24. J. T. Gostick, M. W. Fowler, M. A. Ioannidis, M. D. Pritzker, Y. M. Volkovich, and A. Sakars, *J. Power Sources*, **156**, 375 (2006). 488
25. J. D. Fairweather, P. Cheung, J. St-Pierre, and D. T. Schwartz, *Electrochem. Commun.*, **9**, 2340 (2007). 489
26. T. V. Nguyen, G. Lin, H. Ohn, and X. Wang, *Electrochem. Solid-State Lett.*, **11**, B127 (2008). 490
27. A. Jena and K. Gupta, *Fluid/Part. Sep. J.*, **4**, 227 (2002). 491
28. Y. M. Volkovich, V. S. Bagotzky, V. E. Sosenkin, and I. A. Blinov, *Colloids Surf., A*, **187**, 349 (2001). 492
29. M. J. Martínez, Ph.D. Dissertation, Department of Chemical Engineering, University of South Carolina, Columbia, SC (2008). 493

NOT FOR PRINT!

FOR REVIEW BY AUTHOR

NOT FOR PRINT!

AUTHOR QUERIES — 002905JES

#1 AQ: Did you mean 416 MPa, line 310.

#2 AQ: Please update Ref. 17, line 467.

PROOF COPY [JES-08-1228R] 002905JES